Title

Sea-Level Change in Asia since the Last Glacial Maximum

Author

Tanghua Li

School of Energy and Environment, City University of Hong Kong, Kowloon, Hong Kong SAR, China

Department of Data Science, City University of Hong Kong, Kowloon, Hong Kong SAR, China

Earth Observatory of Singapore, Nanyang Technological University, Singapore, Singapore

Corresponding author

Tanghua Li

Email: Tanghua.LI@cityu.edu.hk

ORCID: https://orcid.org/0000-0003-0501-0155

Manuscript type

This is the author’s preprint of a book chapter, prior to editorial and/or peer review on behalf of the publisher. It has not been peer reviewed.

Intended publication

The manuscript is intended for publication as a chapter in: *Advancements in Coastal Hazards Research in Asia: Identifying Hazards, Managing Risk*, edited by Constance Ting Chua, Hsiao-Wen Wang, and Qinglan Li, Springer (book series: Atmosphere, Earth, Ocean & Space).

It has not yet been published as the Version of Record.

Sea-Level Change in Asia since the Last Glacial Maximum

Tanghua Li[1, 2, 3*]

[1]School of Energy and Environment, City University of Hong Kong, Kowloon, Hong Kong SAR, China

[2]Department of Data Science, City University of Hong Kong, Kowloon, Hong Kong SAR, China

[3]Earth Observatory of Singapore, Nanyang Technological University, Singapore, Singapore

Corresponding author: Tanghua.LI@cityu.edu.hk

Abstract

As a 'far-field' area, distal from former ice sheets, Asia is minimally influenced by the glacial isostatic adjustment process. Therefore, Relative sea-level (RSL) data from Asia, recorded by various geological proxies, provide essential constraints on the history of ice-equavilent sea-level changes. The global mean sea-level has risen over 130 m on average since the Last Glacial Maximum (LGM), significantly altering the paleogeography, landmass distribution, coastal evolution, ecosystems, regional climate and monsoon patterns, as well as the human settlement in the region. Understanding paleo RSL changes is crucial for projections of future sea-level rise and its potential impacts on Asia's densely populated coastal regions.

This chapter introduces the controlling processes behind RSL changes, reviews available RSL proxies in Asia, and discusses the spatial and temporal variability of RSL history since the LGM. Particularly the mid-Holocene highstand, a unique phenomenon that RSL was higher than present-day levels between 7000 and 4000 years ago in the 'far-field' regons, will be illustrated in detail. The mid-Holocene highstand serves as a analogue for future sea-level rise of similar magnitude. This chapter also explores the impact of RSL rise on landmass and human demography, featuring a case study from Southeast Asia that integrates paleogeographic data and population genomics to reveal the earliest documented instance of forced human migration driven by sea-level rise. Additionally, the probability perspectives of future sea level for

Singapore using geological proxies and instrumental measurements since the LGM is provided. It shows that the projected rate of sea-level rise by 2150 under a moderate emissions scenario has only been exceeded (at least 99% probability) during the rapid ice melting events.

Keywords: Sea-level change, Asia, mid-Holocene highstand, paleogeography, human migration.

1 Introduction

Over 70% of the global population (~546 million out of 768 million) residing in low elevation coastal zones (i.e., areas less than 10 m above mean sea level) live in Asia (Nicholls et al., 2021). This makes Asia particularly vulnerable to sea-level rise, underscoring the need for accurate sea-level projections to support effective coastal adaptation, mitigation, and engineering strategies (Nicholls and Cazenave 2010; Fox-Kemper et al. 2021). A prerequisite for producing robust sea-level projections is a thorough understanding of the relationship between sea level and climate forcing, the mechanisms of sea-level change, and their drivers, all of which rely on a comprehensive knowledge of sea-level history (Horton et al. 2018). Most instrumental data only contain records from the mid-to-late twentieth and early twenty-first centuries and captures a single climate mode dominated by anthropogenic forcing (Kopp et al. 2016). Complementing the instrumental records, RSL reconstructions from geological proxies offer insights into longer-term sea-level response to a broader range of climatic forcings and driving mechanisms over centuries to millennia.

This chapter reviews the sea-level change history in Asia since the Last Glacial Maximum (LGM), with an emphasis on its spatial and temporal variability and diverse impacts. It discusses the mechanisms driving relative sea-level (RSL) change and elaborates on the dominant processes involved. Various sea-level indicators, particularly those reported from Asia, are introduced. The deglacial RSL history is presented using data from far-field regions and compared with the latest modelling results. The unique phenomenon of the mid-Holocene sea-level highstand is illustrated with reconstructed RSL data and modelling outputs. Two case studies are included: one documenting forced human migration driven by sea-level rise in Southeast Asia, and another offering a deglacial perspective on future sea level change from Singapore. The chapter concludes with a brief summary and an outlook on future directions in sea-level research across Asia.

2 Mechanisms for relative sea-level change

RSL is defined as the elevational difference between the sea surface and the land at a specific location (Figure 1), whereas global mean sea level (GMSL) refers to the global mean of RSL, due to the change in the volume of the ocean (Gregory et al. 2019). RSL differs from GMSL due to the influences of various global, regional, and local processes that operate over different spatial and temporal scales (Figure 1; Horton et al. 2018).

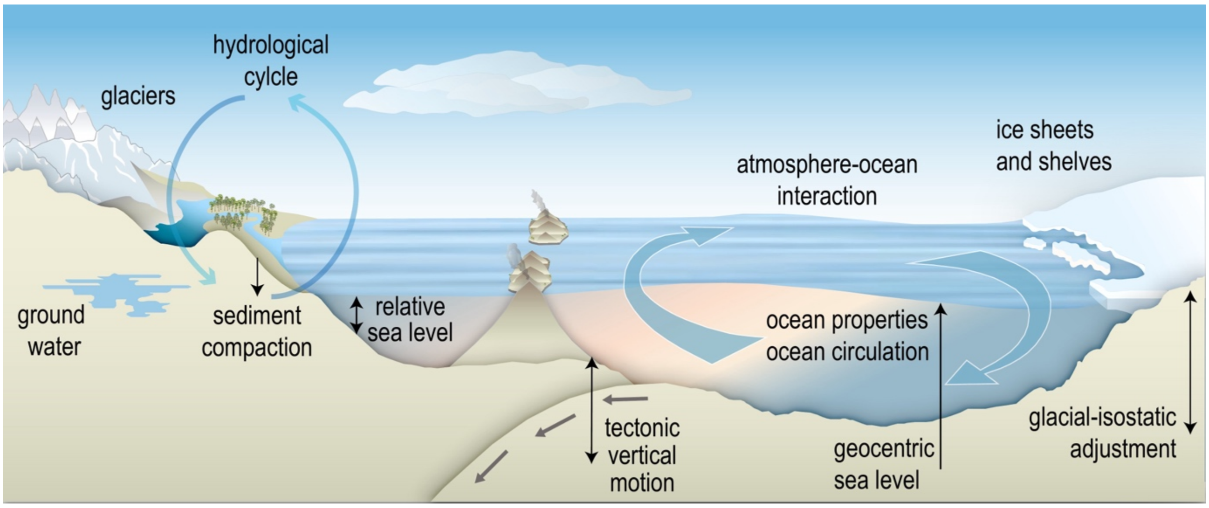

Figure 1. Schematic example of processes driving relative sea-level change. Figure modified after Intergovernmental Panel on Climate Change Fifth Assessment Report (Church et al. 2013).

At the global scale, RSL is primarily controlled by the growth and decay of the continental ice sheets (i.e., glaciation and deglaciation) and the associated viscoelastic response of the solid Earth, a process known as Glacial Isostatic Adjustment (GIA; Peltier et al. 2022). Given the dominant role of GIA in shaping RSL evolution since the LGM, this process will be discussed in detail in the subsequent Section 2.1. In addition to GIA, long-term mantle dynamics, such as mantle flow and mantle convection, drive surface topography changes over million-year timescales and in turn affect RSL patterns.

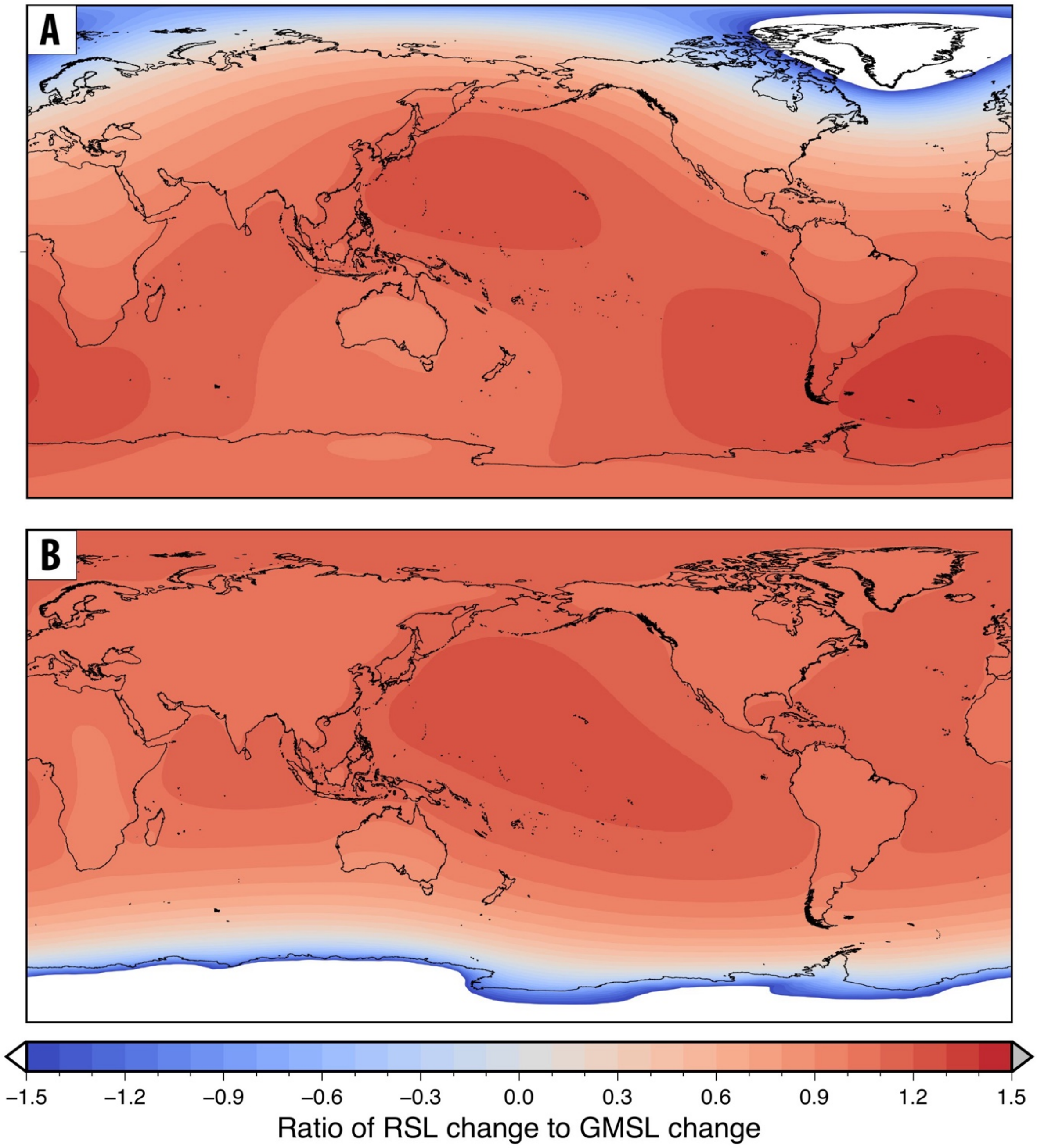

Figure 2. Sea-level fingerprints of ice mass loss from (A) Greenland and (B) Antarctica presented as ratios of relative sea-level (RSL) to global mean sea-level (GMSL) change. Ice mass loss is assumed to occur through uniform thinning across Greenland and Antarctica, with ice sheet geometries from the global ice history model ICE-6G_C (Peltier et al. 2015).

Redistribution of ice and seawater mass induces gravitational, rotational and deformational effects on sea level, commonly referred to as "sea-level fingerprints" (Figure 2; Mitrovica et al. 2001). For example, contemporary melting of Greenland and Antarctica ice sheets generates a gravitational pull reduction that the result in a RSL fall in the near-field (e.g., close to the melting ice sheets), while simultaneously causing a RSL rise in the far-field (e.g., Asia) with magnitude greater than the GMSL signal converted from the melting ice sheets (Horton et al. 2018).

At regional scale (~1000 km), atmosphere/ocean dynamics act as important drivers of RSL change over seasonal, annual, multidecadal, to even longer time scales (Samanta 2025). Key examples include the El Niño–Southern Oscillation, the Indian Ocean Dipole, and the Atlantic Meridional Overturning Circulation, which cause sea-surface height changes due to variations in ocean temperature, salinity, wind, and surface pressure.

At region to local scales (~100 km or less), processes such as sediment compaction, sediment isostatic adjustment, tectonic (co-seismic, post-seismic, inter-seismic), subsidence due to anthropogenic activities (e.g., groundwater extraction, hydrocarbon withdrawal), all affect RSL through their effects on vertical land motion (VLM; Wöppelmann and Marcos 2016). VLM is a critical component in understanding local RSL variability, particularly for future sea-level projections (Shirzaei et al. 2021). VLM has received increasing attention in recent years and will be discussed in detail in the following Section 2.2.

2.1 Glacial Isostatic Adjustment

Proxy climate records (e.g., sea/lake floor sediments, ice cores, fossil pollen and tree-rings) show that there are glacial and interglacial cycles with period of approximately ~120 ka (i.e., thousand years) over the past one million years. During the glaciation phase of a single cycle, typically lasting about 100 ka, large volumes of ocean water are transformed to form ice sheets near the polar regions, leading to a GMSL fall of ~130 m (Figure 3). The reduction in ocean mass causes a slight uplift of the sea floor due to the removal of the hydrostatic load. Meanwhile, the accumulation of ice sheets imposes substantial loading on the surface of the lithosphere, depressing the underlying ground surface by several hundreds of meters and forming a forebulge beyond the ice margins. In contrast, during the deglaciation phase, the ice sheets melt, and water are transferred back to the oceans, causing a GMSL rise of ~130 m. This reloading of the ocean basins results in minor subsidence of the sea floor. Concurrently, the formerly glaciated regions (e.g., near-field) undergo viscoelastic rebound as the ice loads are removed and the forebulge migrates and collapses (Figure 4). The entire process, encompassing the solid Earth's viscoelastic response, changes in the gravitational field, and associated ocean mass redistribution in response to ice sheet growth (i.e., glaciation/loading) and decay (i.e., deglaciation/unloading), is collectively referred to as GIA (Peltier et al. 2022). Due to the high viscosity of the mantle and lithosphere, the GIA process continues for many thousands of years following ice retreat, as evidenced by ongoing surface deformation in formerly glaciated now ice-free regions such as North America and Northern Europe.

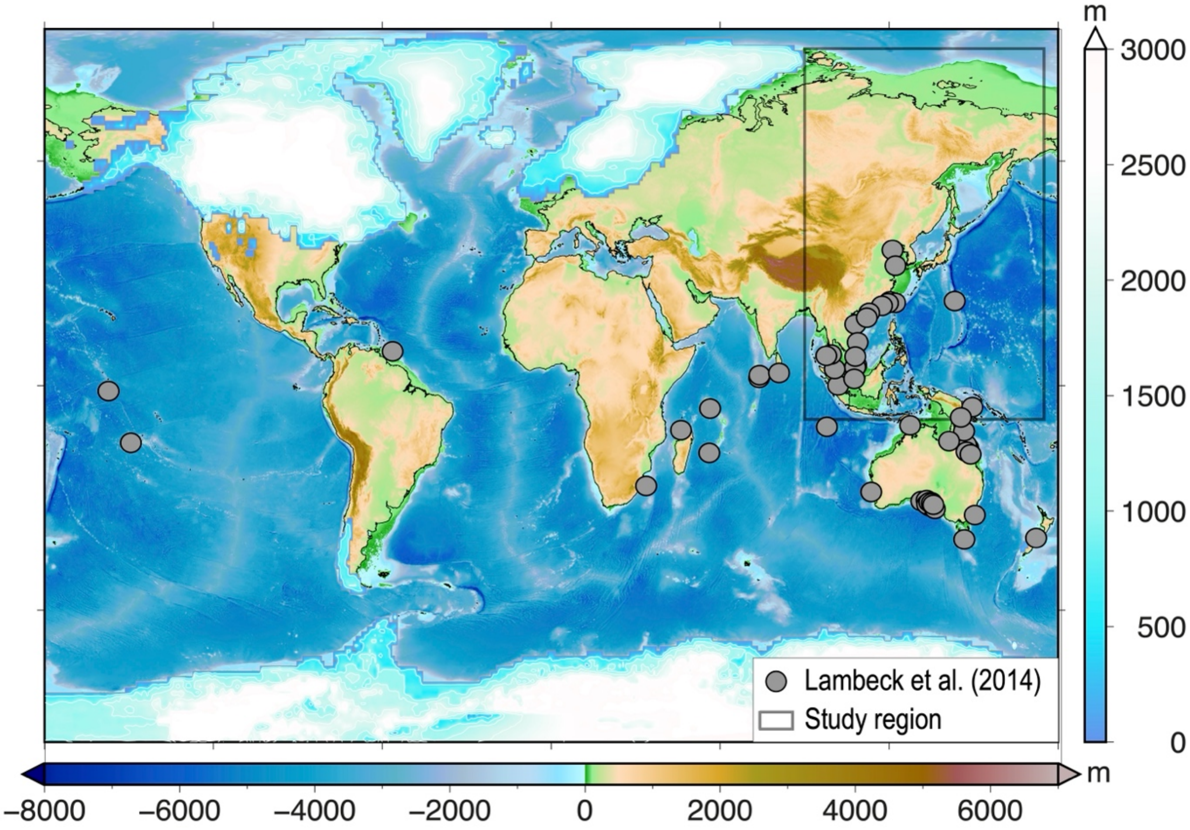

Figure 3. Spatial extent and thickness distribution of ice sheets at the Last Glacial Maximum (LGM) are shown based on the ICE-6G_C global ice history model (Peltier et al. 2015), overlaid on paleotopography at LGM reconstructed using ICE-6G_C and 3D Earth model HetM-LHL140 (Li and Wu 2019). Grey circles represent far-field relative sea-level data included in Lambeck et al. (2014). The grey rectangle highlights Northeast, East, and Southeast Asia, the primary focus of this chapter. The black lines indicate the present-day coastline based on the ETOPO1 global topography model (Amante and Eakins 2009). The green areas extending beyond the present-day coastline represent the landmasses that have been submerged due to sea-level rise from the LGM to present.

The people of Fennoscandia have been aware of the effects of GIA for many centuries, owing to the pronounced land uplift and associated RSL fall signal resulting from the melting of the Fennoscandian Ice Sheet. A notable early example is the *Celsius Rock* on the island of Löfgrundet, Sweden, which has sea-level marks from the years 1731, 1831, and 1931. These marks may represent the beginning of GIA investigations with geodetic techniques (Steffen and Wu 2011). Since then, many scientists collected observational evidence of GIA to better understand the process, laying the foundation for the rapid development of GIA research, particularly in constraining Earh's mantle viscosity from the 1960s on wards. The development of the sea-level equation has evolved over several decades, from a simple concept of ice-equivalent sea level (i.e., total volume of ice mass loss divided by ocean area), to a more comprehensive formulation including geoid change due the redistribution of meltwater and mass within the Earth (e.g., surface deformation, mantle flow), temporal variation of ocean area/shoreline migration, and rotational feedback associated with mass redistribution (Whitehouse 2018).

GIA produces distinct spatial patterns of RSL change since the LGM, primarily governed by the distance from former ice sheets (Figure 4). In the near filed, which was formerly covered by ice sheets, continuous RSL fall has been reconstructed, driven by the dominance of postglacial land uplift over the ice-equivalent sea-level rise. Near the former ice margins, the interplay between vertical surface displacement and ice-equivalent sea-level rise results in a characteristic "fall-rise-fall" RSL pattern, in which the intermediate highstand may exceed present sea level. In the intermediate field, RSL records show a continue rise due to the migration and collapse of the glacial forebulge. In the far field such as Asia, RSL rose from the LGM until the middle Holocene, when it reached a maximum level higher than present (i.e., mid-Holocene sea-level highstand), followed by a gradual RSL fall toward the present day.

The mid-Holocene highstand is a unique phenomenon where regions distal from polar ice sheets experienced RSLs higher than present-day levels between 7,000 and 4,000 years ago. The mid-Holocene highstand is caused by two mechanisms that drive a fall in RSL from mid-Holocene (Figure 4): (1) equatorial ocean syphoning; and (2) continental levering (Li et al., 2023; Mitrovica & Milne, 2002). Equatorial ocean syphoning describes the migration of water from far-field regions into areas vacated by forebulge collapse and subsidence at the periphery of deglaciation centers to maintain dynamic equilibrium (Mitrovica & Peltier, 1991). Continental levering links to VLM of continental margins due to the increasing ocean loading caused by rising sea levels, which induces a subsidence of offshore regions and an uplift of onshore regions (Mitrovica & Milne, 2002).

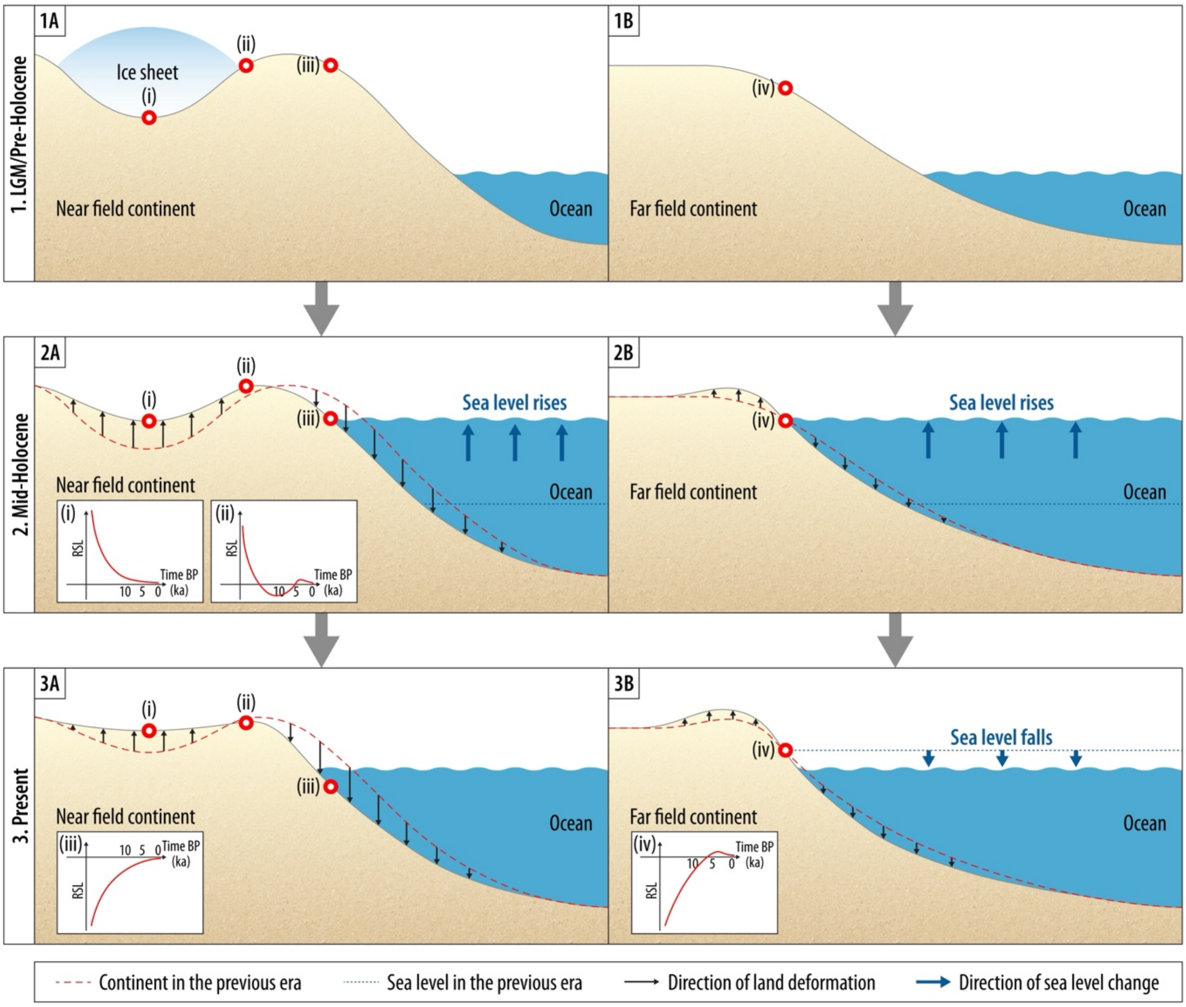

Figure 4. Schematic illustration of the Glacial Isostatic Adjustment process at three key time periods: Last Glacial Maximum (LGM)/pre-Holocene, mid-Holocene, and the present. The schematic highlights two mechanisms responsible for the mid-Holocene sea-level highstand: **A** equatorial ocean syphoning and **B** continental levering. Insets i-iv demonstrate representative patterns of relative sea-level change from the LGM till present at four distinct locations: (i) near-field close to former ice sheet center (e.g., Hudson Bay, Canada), (ii) near-field close to the former ice sheet margin (e.g., Andoy, Norway), (iii) intermediate-field near the forebulge (e.g., New Jersey, U.S.), (iv) far-field (e.g., Singapore). Figure adapted from Li et al. (2023), with permission from Elsevier.

The simulation of GIA process requires two fundamental inputs, an ice model and an Earth model. The ice model describes the spatiotemporal evolution of ice-sheet extent and thickness over a glacial and interglacial cycle (e.g., ICE-6G_C, Figure 3), while the Earth model defines the internal structure of the Earth, including the elastic properties and rheological parameters (e.g., viscosity). For modelling approaches, the conventional spectral normal mode method has been widely employed for simulating GIA in a 1D case (i.e., laterally homogeneous). However, more numerical methods, such as finite-element method (Wu 2004), spectral finite-element method, and finite-volume method (Latychev et al. 2005), have also been developed. Particularly, to consider lateral variations in lithospheric thickness and lateral variations in mantle viscosity (i.e., 3D/laterally heterogeneous), finite-element and finite-volume methods have become increasingly adopted over the last two decades. These 3D approaches have been shown to improve the fit with GIA observations, including RSL data (Li et al. 2020, 2022), highlighting the importance of incorporating 3D Earth structure in GIA modelling (Kuchar et al. 2019).

GIA model predictions are usually compared with GIA-related instrumental observations to constrain the input parameters, including observations of surface deformation (e.g., Global Navigation Satellite System/GNSS, satellite altimetry, tide gauges) and gravity-rate-of-change (e.g., Gravity Recovery and Climate Experiment/GRACE). However, there are obvious non-uniqueness issues in constraining GIA model when solely use present-day observations. For example, a larger ice loss at an earlier time (e.g., 10 ka BP) can result in the same present-day uplift rate as a smaller ice loss at a younger time (e.g., 5 ka BP). Similarly, a combination of greater ice loss and weaker mantle rheology can produce present-day uplift rates equivalent to those generated by smaller ice loss paired with a stronger rheology (Whitehouse 2018). Therefore, to largely resolve such ambiguities, paleo proxy data are essential for constraining and validating GIA models. These data include records of past ice-sheet extent (e.g., moraines, grounding zone wedges, and glacial geomorphology), paleoshoreline reconstructions, and most importantly the paleo RSL data. Continued efforts to generate new RSL records (e.g., Engelhart et al. 2011; Xiong et al. 2020), compile standardized RSL databases (e.g., Khan et al. 2019), and assign robust quality assessments (e.g., Tan et al. 2023), have significantly improved the capability to constrain GIA models (e.g., Kuchar et al. 2019; Li et al. 2022) and reduce the modelling uncertainty (e.g., Li et al., 2020).

2.2 Vertical land motion

VLM is caused by various natural and anthropogenic processes, including mantle dynamic tomography, GIA, tectonics, sediment loading and compaction, and subsidence from resource (e.g., groundwater, hydrocarbon) extraction. Short-term (annual to decadal) VLM signals have been estimated from instrumental measurements such as satellite altimetry, Interferometric Synthetic Aperture Radar (InSAR), tide gauges, and GNSS.

In recent year, InSAR has become an increasingly valuable tool to monitor the VLM due to its extensive spatial coverage and high spatial resolution. For example, Tay et al. (2022) used six years of InSAR data to estimate the local relative VLM for the 48 largest coastal cities globally. They revealed significant spatial variability in VLM rates both within cities and across different cities and demonstrated that VLM is generally underestimated in the sea-level projections of the Intergovernmental Panel on Climate Change (IPCC) Sixth Assessment Report (AR6) (Fox-Kemper et al. 2021). However, InSAR typically provides relative VLM measurements referred to a reference point, the results must be transformed into a regional or global reference frame (e.g., International Terrestrial Reference Frame 2014) if one wants to compare with other geodetic data (e.g., GNSS).

Tide gauge records have also been used, such as in IPCC AR6, to derive the VLM signal. However, tide gauges measure changes in sea level relative to the land where they are installed (Figure 5), including changes in both land height and sea surface height. The latter includes the sea-level contribution from non-VLM sources such as thermal expansion, mass input from melting ice sheets and glaciers, and changes in land water storage. Consequently, relying solely on tide gauge data to estimate VLM can introduce systematic biases (e.g., Li et al. 2024). Moreover, many gauges are located in port facilities where wharf removal, development, and/or extensions occur, the datum history of the tide gauge can be problematic (e.g., Ng et al. 2025). Where possible, tide gauge records should be subtracted by satellite altimetry data to separate the VLM signals (Figure 5; Peng et al. 2024), although the differenced altimetry-tide gauge approach is still developing and is limited by the broad spectrum of error sources.

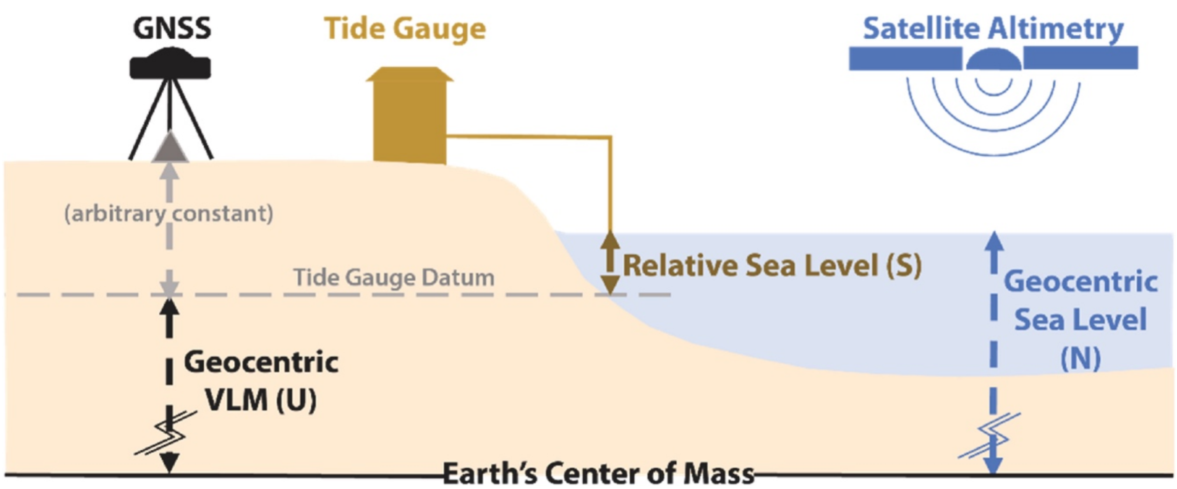

Figure 5. Schematic illustration of instrumental observations from Global Navigation Satellite System (GNSS), tide gauge, and satellite altimetry. Figure adapted from Peng et al. (2024), with permission from Elsevier.

GNSS data have been widely used to estimate the VLM signal since the mid-1990s, when continuous Global Positioning System (GPS) networks and precise geodetic positioning techniques became available. GNSS measurements on surface deformation are essential to validate and correct other observations. Nevertheless, they are limited by the station spatial coverage (e.g., mainly along the active faults, subduction margins) and temporal time span, particularly lack of stations along coastal regions (Hammond et al. 2021).

Importantly, all instrumental observations can only record VLM information in the last few decades, while the processes that drive VLM often operate beyond instrumental era. To better understand those VLM processes, it is necessary to estimate the long-term (multi-centennial to millennial scale) rates of VLM, which can be derived from paleo proxy data. In tropical regions, fossil corals (e.g., microatolls) have been used to reconstruct tectonically driven VLM. More broadly, paleo RSL data, particularly late-Holocene RSL data, supported by GIA models, have been used to derive long-term VLM signal in the U.K., Atlantic and Pacific coasts of the U.S., Oceania, Eastern Mediterranean, and Adriatic coast of Croatia. Recently, Li et al. (2024) estimated the long-term VLM from northern Spain using late-Holocene RSL data and 3D GIA models, which was validated with local instrumental observations. They showed that the VLM signal used in IPCC AR6 sea-level projections was underestimated in the region. Their study highlights the importance of estimating both long-term and short-term VLM signals, particularly for sea-level projection purposes.

3 Sea-level indicators

Sea-level indicators are in situ geological, biological, morphological, or archeological features whose formation was controlled or influenced by past sea-level and can provide reliable estimates of past changes in RSL with quantified uncertainty (Shennan et al. 2015). These indicators are typically characterized by four fundamental attributes (Khan et al. 2019): (1) geographic location, defined by precise geographic coordinates measured to a national or internation convention (e.g., longitude and latitude); (2) age of formation, usually determined through radiometric dating techniques such as radiocarbon or U-series dating; (3) elevation, expressed relative to a modern tidal datum; and (4) indicative meaning, which describes the relationship between the indicator and sea level, encompassing both a reference water level (central tendency) and an indicative range (vertical range distribution relative to tidal levels).

Based on their indicative meaning, sea-level indicators are commonly classified into sea-level index points (SLIPs) and limiting data. SLIPs constrain the past position of RSL in both time and space, with defined vertical and chronological uncertainties. In contrast, limiting data provide either an upper bound (terrestrial or freshwater limiting data points) or a lower bound (marine limiting data points) on past RSL positions, also with quantified uncertainties.

In Asia, a wide variety of sea-level indicators have been documented across different latitudes and environments. In tropical and subtropical latitudes, fixed biological indicators–organisms that are attached to hard substrates and whose living range, or the upper part of it, is closely associated with sea level (Shennan et al. 2015)–are extensively used to reconstruct past RSL changes. These indicators include, but are not limited to, corals (e.g., coral reefs and microatolls), oysters, vermetidae, and balanidae. In addition, other sedimentary and geomorphic features such as mangroves peats, beachrocks, beach ridges, and tidal notches are commonly used sea-level indicators in low latitude coastal environments. For mid- to high-latitude regions, geological sediment indicators, particularly saltmarsh peat, are widely used for past sea level reconstruction.

4 Deglacial sea-level change in Asia

The understanding of deglacial RSL change is mainly based on records from several well-studied far-field sites, such as Barbados, Tahiti, Bonaparte Gulf, Papua New Guinea, the Great Barrier Reef, and Sunda Shelf. Compiled far-field RSL datasets, including those from Asia, show the GMSL was over 130 m lower than present during the LGM (~26-21 ka BP), when the global grounded ice volume reached its maximum extent (Lambeck et al. 2014). At the LGM sea level lowstand, extensive landmass in Asia were exposed above sea level (Figure 3), such as the central Sunda shelf and continental shelves along the coasts of China and East Siberia.

Following the LGM, the onset of deglaciation initiated the GMSL rise driven by the melting of continental ice sheets with fluctuated rising rates (Figure 6). The most notable periods of rapid sea-level rise are the Meltwater Pulse (MWP) events, which are triggered by rapid influx of meltwater resulting from ice-sheet collapse and the drainage of ice-dammed lakes and subglacial lakes, such as the MWP1A (~14.5 – 14 ka BP) and MWP1B (~11.5 – 11 ka BP). MWP1A was first identified through radiocarbon-dated fossil coral reef records from Barbados and later supported by further evidence from Tahiti, the Sunda Shelf, and the Great barrier Reef, indicating it is a global scale phenomenon. MWP1A is attributed to rapid melting of Northern Hemisphere ice sheets, particularly the Laurentide and Eurasian ice sheets (Lin et al. 2021).

MWP1B was also first recognized in the Barbados coral records and subsequently supported by data from the Western pacific and polar Arctic. However, it remains debated about its global significance, as the magnitude of sea-level rise associated with WMP1B is much smaller in the Great Barrier Reef and absent from the Tahiti record. Nevertheless, recent modelling study suggests that MWP1B could result from meltwater contribution from Laurentide and Antarctica ice sheets (Velay-Vitow et al. 2024).

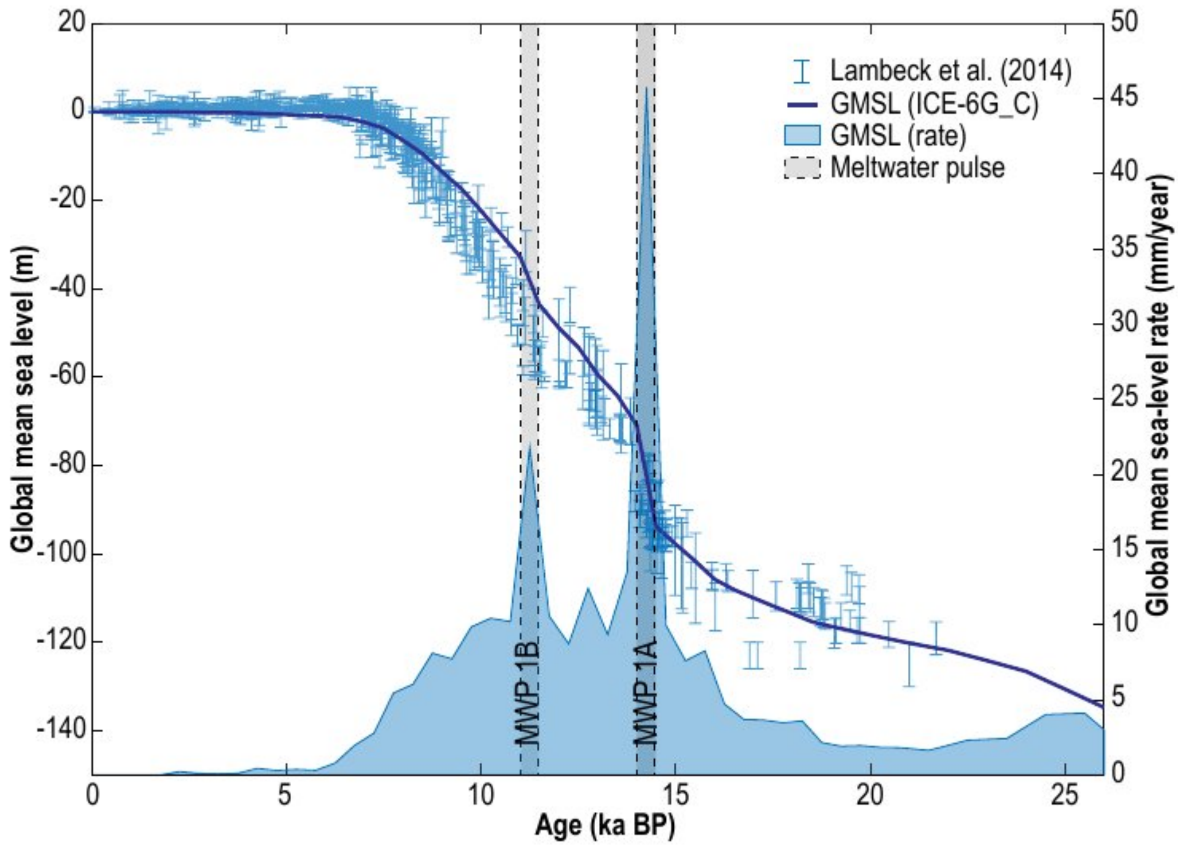

Figure 6. Relative sea-level data from Lambeck et al. (2014) (at sites shown in Figure 3) and magnitudes and rates of global mean sea-level change derived from ICE-6G_C model. The timing and magnitude of Meltwater Pulse (MWP) 1A and 1B evets are highlighted in the figure. Figure modified after Kim et al. (2023), licensed under CC BY 4.0.

The GMSL predictions from the global ice history model ICE-6G_C (Peltier et al. 2015) generally match the far-field RSL data compiled by Lambeck et al. (2014) within the uncertainty range, although misfits persist from the end of MWP1A to early Holocene (Figure

6). The model predicts a GMSL of ~130 m since 26 ka BP (i.e., LGM in ICE-6G_C) and reconciles the MWP1A and MWP1B events. Between 14.5 and 14 ka BP, the GMSL rose from -93.8 m to -70.9 m at a rate of 46 mm/yr, while between 11.5 and 11 ka BP, GMSL rose from -43.6 m to -32.7 m at a rate of 22 mm/yr.

5 Landmass change in Southeast Asia and prehistoric human migration

Southeast Asia has undergone substantial changes in landmass and topography since the LGM due to RSL rise (Figures 3 & 6). Shaw et al. (2023) quantitatively reconstructed the paleo-topography change of the Sunda Shelf region at 0.5 ka intervals to capture the spatial and temporal evolution of land area and lateral shoreline migrations in response to post-LGM sea-level rise. Their reconstruction employed the global ice history model ICE-6G_C (Peltier et al. 2015), the 3D Earth model HetM-LHL140 (Li and Wu 2019), and the present-day topography model ETOPO1 (Amante and Eakins 2009). Then those reconstructions were used to calculate land area differences and lateral shoreline migration rates compared to the present-day topography (Figure 7).

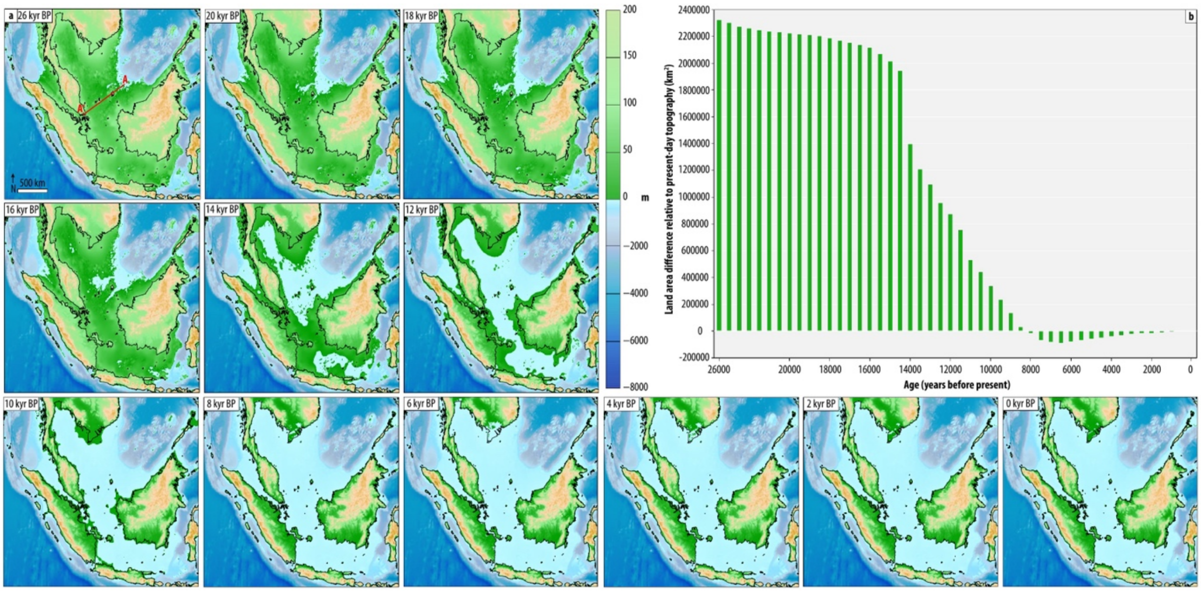

Figure 7. **a** Paleotopographic maps showing landmass change as rising sea level flooded the Sunda Shelf since the Last Glacial Maximum (i.e., 26 ka BP in ICE-6G_C). b Calculated land area differences relative to the present-day topography (Amante and Eakins 2009). Red transect line A-A' in 26 ka BP panel used to calculate lateral shoreline migration rates. Figure adapted from Shaw et al. (2023), licensed under CC BY 4.0.

At the LGM, the exposed land area of the Sunda Shelf exceeded present-day conditions by approximately 2.3 million km^2, nearly doubling the modern exposed landmass in the region (Shaw et al. 2023). This implies that roughly 50% of the Sunda Shelf's land area has been submerged due to sea-level rise since the LGM. The RSL rise drove average lateral shoreline migration at a rate of ~57 m/yr, with peak rates over 300 m/yr during the MWP1A (Figure 7).

Notably, Southeast Asia is the only region globally that experienced major reductions in the land area during the transition from the LGM and meanwhile, has continuously been occupied by today's indigenous human populations. Therefore, it provides a model testbed to investigate the impact of paleoclimate changes on past and present human demography. Previous studies have suggested that post-LGM climate changes affected populations living in the Sundaland, largely based on mitochondrial DNA or Y chromosome data, and genotyping data. However, these data provided limited insights into detailed population structure. In contrast, whole-genome sequence datasets provide a more accurate and unbiased reconstruction of demographic histories.

To this end, Kim et al. (2023) inferred the human population history in Southeast and South Asia using 763 high-coverage whole-genome sequencing datasets from 59 ethnic groups. The high-coverage whole-genome data were generated by the GenomeAsia 100K consortium (Wall et al. 2019) and only individuals native to Southeast and South Asia were selected with European populations as reference groups. Principal component analysis and admixture modelling were used to investigate population structure and admixture. The authors reconstructed the admixture history, estimated the timing of admixture events and timing of population splits, and inferred effective population sizes and population densities through time.

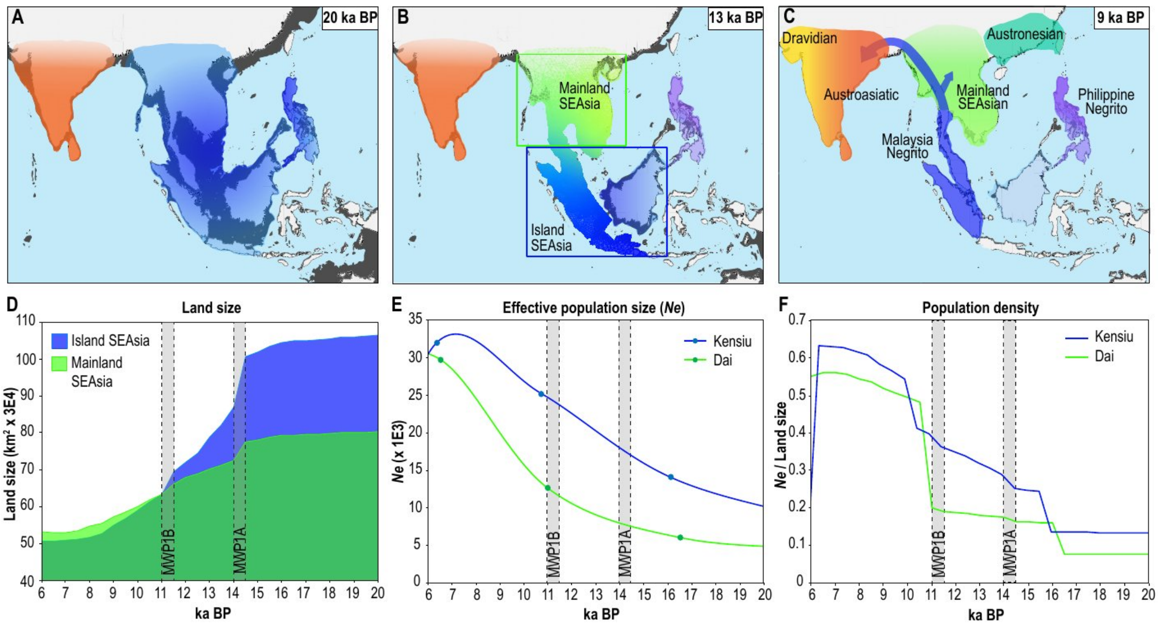

Figure 8. Landmass size change and reconstructed demographic history across Southeast Asia since the Last Glacial Maximum. Kim et al. (2023) hypothesized population migration and splits on the map along with the sea-level changes. The geographic regions inhabited by the ancestral populations are suggested based on the current locations of their descendants and represented as colored shading in the map. The changes in inhabitancies over time are reconstructed based on the demographic history estimates. **A** 20 ka BP, the ancestral population of Southeast Asians likely inhabited Sundaland. The ancestors of the Austroasiatic speakers in South Asia might have occupied the Indian subcontinent. **B** 13 ka BP after MWP1A, the ancestral Southeast Asians split into three populations. **C** 9 ka BP after MWP1B, a population split occurred between Mainland Southeast Asians and Austronesians. The blue arrows represent the admixture of the Malaysian Negritos with South Asians and Mainland Southeast Asians and do not represent the migration route. South Asians split into two or three populations around this time. **D** Estimated size of landmass of Island (blue) and Mainland Southeast Asia (green) since 20 ka BP as their regions are indicated in **B**. **E** The fitted curves of Multiple Sequentially Markovian Coalescent estimates of effective population size over time for Kensiu and Dai populations, as representatives of Malaysian Negritos and Mainland Southeast Asians from Island and Mainland Southeast Asia, respectively. **F** Estimated population density over time since 20 ka BP for the two regions indicated in **B**. More details on population estimation may refer to Kim et al. (2023). Figure adapted from Kim et al. (2023), licensed under CC BY 4.0.

Through integrating these demographic reconstructions with paleo-topographic maps of Southeast and South Asia, Kim et al. (2023) assessed the impact of sea-level rise on pre-historic human populations in equatorial regions (Figure 8). Their results suggest that MWP1A and MWP1B promoted multiple population splits by inundating large areas of Sundaland, flooding land bridges between Malay-Thai Peninsula, Sumatra, Borneo, and Palawan (Figure 8). The fragmentation also reduced forest cover and amplified the regional monsoon system. Following these population splits, there was a population expansion (Figure 8 E & F) when the rates of sea-level rise decreased and created a more favorable environment. The stabilization of sea level after WMP1B led to the formation of extensive coastal wetlands and peatlands, enhancing coastal productivity and increasing the availability of nutrition-rich food for human consumption. Kim et al. (2023) demonstrated the earliest documented example of forced human migration driven by sea-level rise, underscoring the importance of integrating geological and genomic data to understand human responses to environmental change.

6 Mid-Holocene sea-level highstand

The mid-Holocene sea-level highstand has been recognized for decades in far-field regions, including Asia (e.g., Woodroffe and Horton 2005). However, the timing, magnitude, and spatial variability of the highstand across Asia are poorly constrained due to limited understanding of the controlling parameters in GIA modelling on producing the highstand and scarcity of available RSL data (Figure 9).

Recently, Li et al. (2023) conducted a comprehensive investigation on GIA modelling of the mid-Holocene sea-level highstand in Singapore and Southeast Asia. Using the ICE-6G_C (VM5a) as a reference model, they systematically tested a wide range of GIA parameters that affect the highstand characteristics. According to the reference model, the highstand first emerged along the Malacca Strait, east coast of Sumatra and southwest coast of Borneo at ~8.5 ka BP with a magnitude of 0.1-1 m. Then, the highstand expanded outwards and reached the maximum (~4.5 m) in Southeast Asia at 6.5 ka BP and decreased thereafter with a consistent highstand distribution pattern (Figure 10).

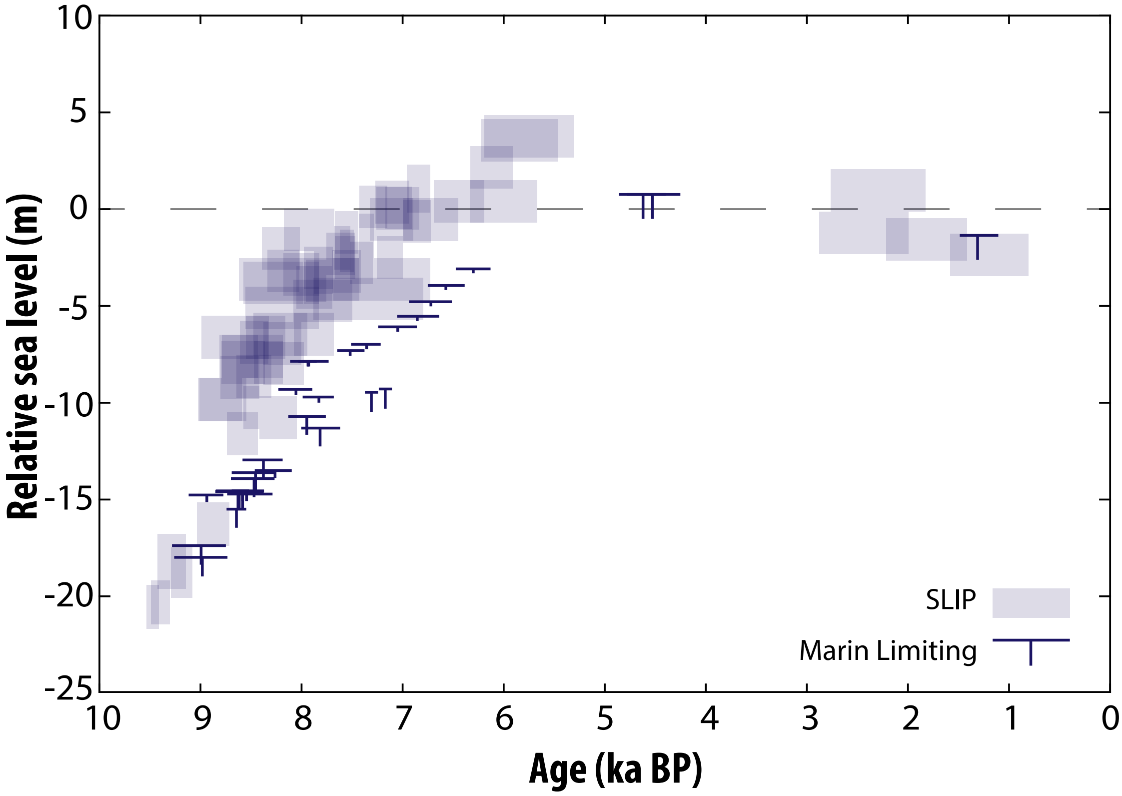

Figure 9. Relative sea-level (RSL) data, including sea-level index points (SLIPs) and marine limiting data, from Singapore. The grey horizontal dashed line represents zero value line. RSL data are from Chua et al. (2021).

At the peak highstand timing (i.e., 6.5 ka BP), highstands existed across all regions of Sundaland and the highstand contours follow the coastlines of outer Sundaland (Figure 10). The pattern of highstand (i.e., positive RSLs) on land and negative RSLs offshore is consistent with the highstand patterns revealed in other far-field regions (e.g., Australia, South America). Peak highstand magnitudes exceeding 4 m are predicted in the southern Malacca Strait and along the east coast of Sumatra. The highstand magnitude declines westwards and southwards and reaches ~0.5 m or less near the northern tip of Aceh and ~2 m along the south-central coast of Java, respectively. The highstand is ~3 m along the coast of Borneo and east coast of Malay-Thai Peninsula, ~3.5 along the northern coasts of the Gulf of Thailand and decreases westwards and eastwards.

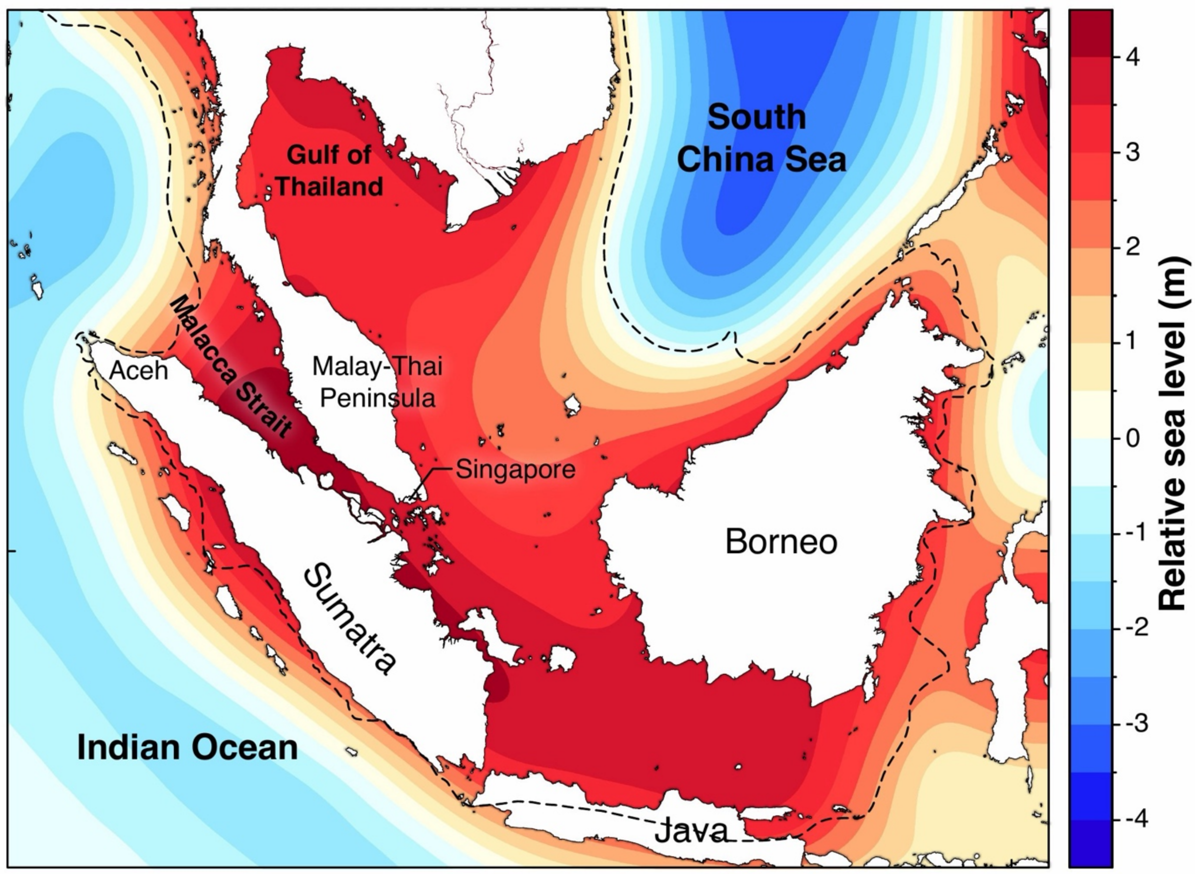

Figure 10. Relative sea-level (RSL) predictions of Glacial Isostatic Adjustment model ICE-6G_C (VM5a) in Southeast Asia at 6.5 ka BP. Positive RSL means above present-day sea level. The dotted line indicates the boundary for Sundaland. Figure adapted from Li et al. (2023), with permission from Elsevier.

Sensitivity tests revealed that the highstand is relatively insensitive to variations in lithospheric thickness, but sensitive to changes in upper and lower mantle viscosities, particularly when the lower mantle viscosity is $<1.0 \times 10^{22}$ Pa s (Li et al. 2023). The highstand along coasts of inner Sundaland, including west and east coasts of Malay-Thai Peninsula, east coast of Sumatra, and west coast of Borneo, are sensitive to upper (1D) and lower (both 1D and 3D) mantle viscosities. Earth model variation only affects the magnitude of the highstand unless extraordinary low upper mantle viscosity is used ($<4.0 \times 10^{19}$ Pa s), which leads to a shift of the highstand towards present and an absence of the highstand when the upper mantle viscosity is $<1.0 \times 10^{19}$ Pa s. On the contrary, ice model variation changes both the timing and magnitude of the highstand. Delaying the ice melting history will shift the timing of the highstand later and result in a lower highstand magnitude.

To guide future RSL data collection efforts to better constrain the highstand, Li et al. (2023) produced a mid-Holocene highstand "treasure map" that identifies regions that are very likely (≥90% probability) to have highstand record preservation (Figure 10). Unlike traditional sensitivity maps, which only highlight regions with model sensitivity that are greater than the observational uncertainty but do not evaluate the likelihood of sedimentary record preservation, the "treasure map" considers the paleo topography evolution and accommodation space. The authors ran an ensemble of 1D and 3D GIA models and calculated the mean and standard deviation of RSL predictions. Assuming the highstand prediction uncertainties are normally distributed with the mean and standard deviation as calculated from the GIA model ensemble, they estimate the probability distribution of having a highstand during the Holocene period in the region.

The resulting mid-Holocene highstand "treasure map" shows that northeast coast and central west coast of Malay-Thai Peninsula, east coast of Sumatra, north coast of Java, and southwest coast of Borneo are very likely (≥90% probability) to have the mid-Holocene highstand preservation (Figure 11). They validated their mid-Holocene highstand "treasure map" with a peak highstand database they compiled from published highstand records. The locations of the highstand records from sedimentary materials and fixed biological indicators match well with the areas showing highstand preservation denoted in the "treasure map". Notably, the absence of highstand records in Aceh, Sumatra, reported by Kelsey et al. (2015), is consistent with low-preservation probability predicted by the "treasure map".

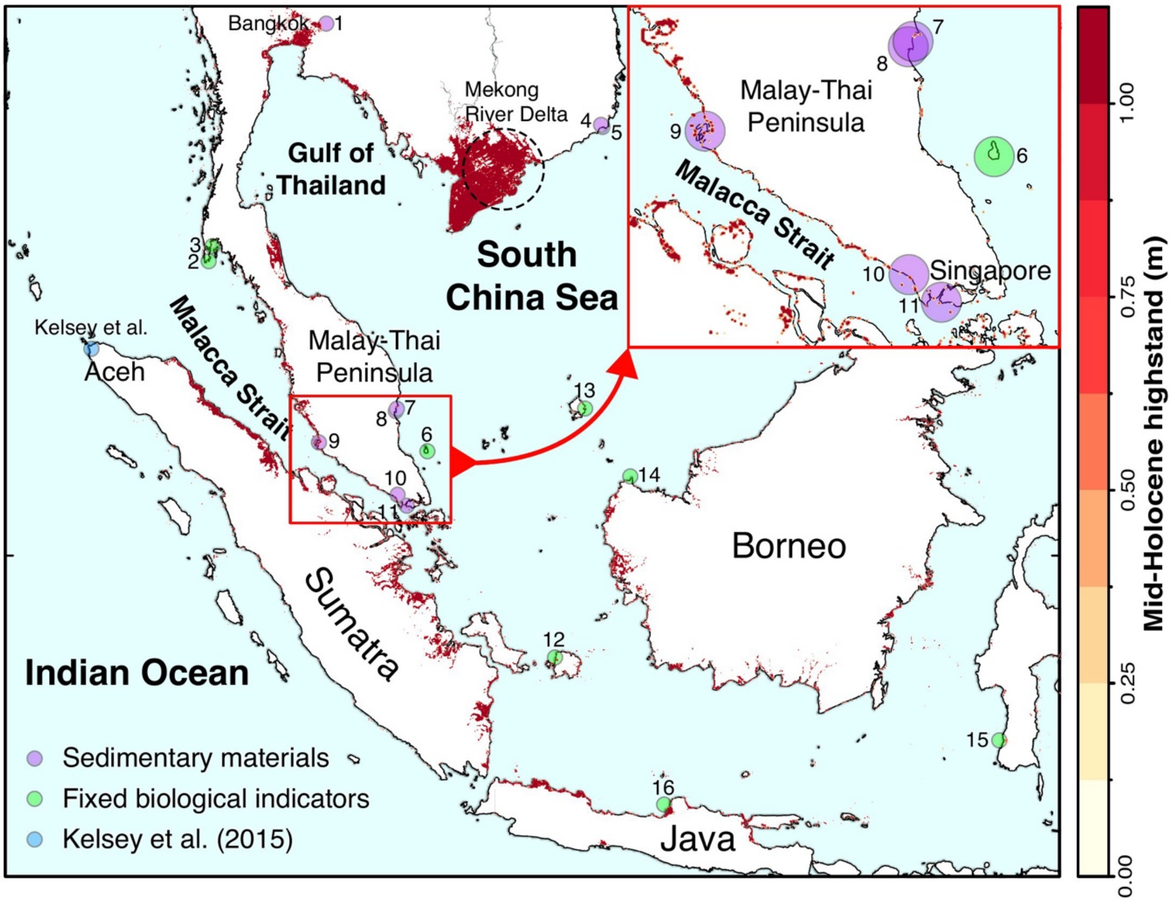

Figure 11. "Treasure map" of the mid-Holocene sea-level highstand in Southeast Asia. The red dots and scatters represent the regions that are very likely (≥90% probability) to have mid-Holocene sea-level highstand record preservation considering topography change and accommodation space across Southeast Asia. The legend on the right indicates the predicted highstand magnitude (e.g., dark red dots indicate the region with predicted highstand magnitude over 1 m; yellow/orange dots indicate the regions with predicted highstand magnitude less than 0.5 m, such as part of northwest coast of Borneo). The purple and green dots represent published highstand records derived from sedimentary materials and fixed biological indicators (e.g., corals, oysters and calcareous algae), respectively. The sea-level reconstruction site in Aceh from Kelsey et al. (2015) showing no evidence of a highstand is shown in blue dot. Figure adapted from Li et al. (2023), with permission from Elsevier.

Note that the "treasure map" does not consider the non-GIA local and regional factors that may affect the preservation and elevation of the highstand records, such as tectonics, subsidence, erosion and deposition, and post-depositional change. Although RSL data from such non-GIA signal affected regions (e.g., Mekong River Delta, Chao Phraya Delta) may not be ideal for validating GIA models and "treasure map", comparison of GIA highstand predictions and RSL data from these regions can reveal the local/regional subsidence/uplift signals (Li et al. 2024).

The approach developed by Li et al. (2023) for producing a mid-Holocene highstand "treasure map" can be applied to other regions globally and extended to map targeted RSL data for any specified time point/period.

7 Deglacial perspectives of future sea level: A case study from Singapore

Singapore, a small (~730 km^2) low-laying island nation located in the equatorial region, is particularly vulnerable to sea-level rise. Accurate sea-level projections are therefore essential for informing effective mitigation and adaptation policies. However, generating reliable sea-level projection requires a comprehensive understanding of the underlying drivers of sea-level change across multiple temporal scales. Paleo sea-level records, particularly those extending beyond the instrumental era, provide an important analogue for investigating past sea-level variability and its associated impacts. These records also contextualize future sea-level projections by revealing the environmental conditions under which similar changes occurred in the geological past.

To achieve this, Shaw et al. (2023) integrated instrumental observations and Holocene geological reconstructions of RSL from Singapore with the pre-Holocene RSL data from the Sunda Shelf to synthesize a complete RSL evolution history of Singapore from the LGM to the present. An Error-In-Variables Integrated Gaussian Process (EIV-IGP) model was subsequently applied to estimate magnitudes and rates of RSL change over time. They then incorporated the sea-level projection from IPCC AR6 for Singapore and compared them with the EIV-IGP model outputs, allowing for the estimation of probability distribution function that indicate when and how likely the projected rates of sea level rise under different scenarios were exceeded in the past.

The averaged records from the four longest tide gauges in Singapore: Sembawang, Tanjong Pagar, Raffles Lighthouse, and Sultan Shoal, were used to quantify sea-level change during the 20th and 21st centuries. These were supplemented by SLIPs derived from coral microatolls from Mapur Island, Indonesia, which had been used to extend the tide gauge records (Majewski et al. 2022). Additional SLIPs based on mangrove intertidal peats from Singapore (Chua et al. 2021) and SLIPs from central Sunda Shelf (Hanebuth et al. 2000) were also incorporated. To consider the spatial variability in RSL between Singapore and central Sunda Shelf, an additional vertical uncertainty was introduced based on ICE-6G_C (HetM-LHL140) GIA model predictions at both locations. The synthesized RSL dataset was used as input to run the EIV-IGP model at 250-year intervals, producing continuous estimates of RSL and its rate of change both with 95% credible intervals (Figure 3 of Shaw et al. (2023)).

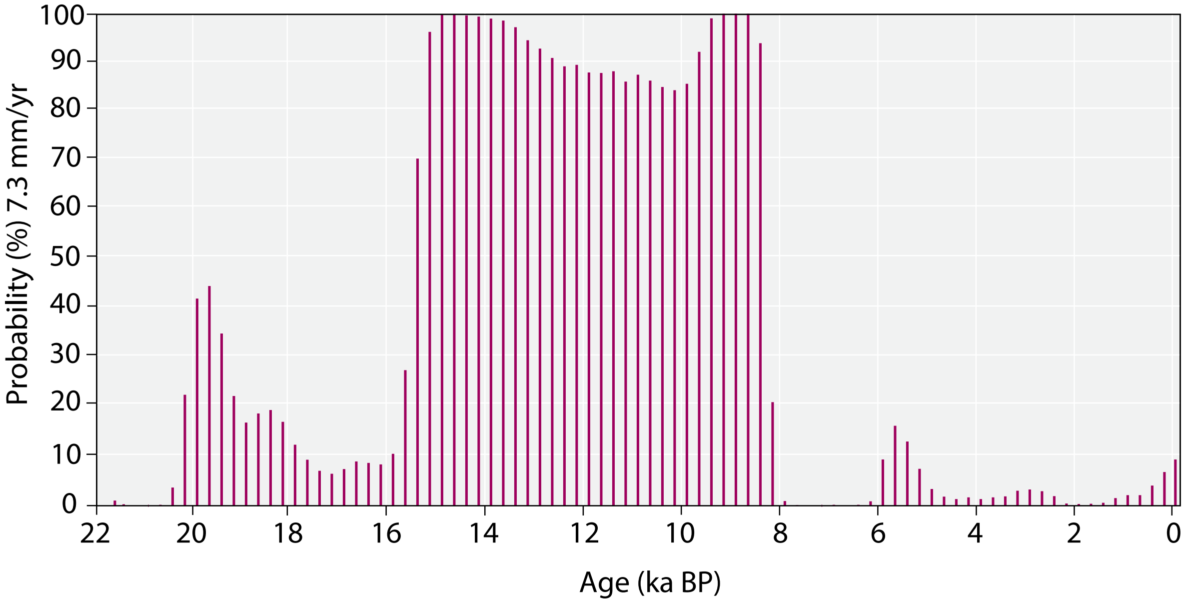

Figure 12. Probability (%) of rates of relative sea-level (RSL) rise during the geological past based on 250-year average bins exceeding 7.3 mm/yr that reflect projected (50th percentile) rate of RSL rise by 2150 under SSP2-4.5 scenario in Singapore. Figure adapted from Shaw et al. (2023), licensed under CC BY 4.0.

According to IPCC AR6, under the moderate emissions shared socioeconomic pathway scenario (SSP2-4.5), RSL is projected to rise 0.95 m (likely range: 0.62-1.4 m) at a rate of 7.3 mm/yr (4.4-11.6 mm/yr) by 2150 in Singapore. Comparison with the rates derived from the EIV-IGP model indicates it is virtually certain that rates of RSL exceeded 7.3 mm/yr only during two brief deglacial periods: 15-14 ka BP and 9.25-8.75 ka BP (Figure 12), while rates over the last ~8 ka BP were unlikely to have surpassed 7.3 mm/yr. This highlights that, even under a moderate emissions scenario (i.e., SSP2-4.5) considered plausible under current global trajectories, future sea-level rise may reach rates unprecedented in the last eight millennia. The Singapore case study underscores the urgency of making effective mitigation efforts and developing reliable adaptation strategies to tackle accelerating sea-level rise.

8 Conclusions and outlook

Research on sea-level change in Asia has been ongoing for several decades and covers a wide range of topics, including sea-level reconstructions based on proxy records, shoreline migration due to sea-level variations, topographic and geomorphological evolution, demographic impacts of sea level, and the investigation of specific RSL features such as MWP events and the mid-Holocene highstand. These studies aim to improve understanding of the regional sea-level history, its driving mechanisms, and associated environmental and societal impacts. It is now well understood that sea-level change is driven by multiple processes operating across different spatial and temporal scales. GIA dominates the post-LGM RSL change in Asia and its simulation involves both ice and Earth models. VLM affects the local and regional RSL, deviating from the GMSL. The sea-level history can be reconstructed using a variety of RSL indicators, which need four attributes about the sample: location, age, elevation, and indicative meaning.

Sea-level was over 130 m lower than present at the GLM and subsequently rose during deglaciation, marked by MWP1A and MWP1B events. Sea-level rise submerged ~2.3 million km^2 landmass in Southeast Asia since the LGM and broke land bridges connecting Malay-Thai Peninsula, Sumatra, Borneo, and Palawan, forcing the prehistoric human to migrate followed by demographic expansion under more stabilized sea level since the early Holocene.

The mid-Holocene highstand covered whole Southeast Asia at ~6.5 ka BP with peak highstand over 4 m centered along the Malacca Strait and east coast of Sumatra. The highstand timing is mainly controlled by the ice model (i.e., ice-equivalent sea level), while the highstand magnitude is affected both by the ice and Earth models. To guide future RSL data collection efforts to better constrain the highstand characteristics, a mid-Holocene highstand "treasure map" is produced, identifying that northeast coast and central west coast of Malay-Thai Peninsula, east coast of Sumatra, north coast of Java, and southwest coast of Borneo are very likely (≥90%) to have highstand record preservation.

A RSL record was synthesized in Singapore from the LGM to present combining instrumental and geological records and magnitudes and rates of RSL change were estimated using an EIV-IGP model. Comparing these EIV-IGP outputs with IPCC AR6 projections revealed that, under a moderate emissions scenario (SSP2-4.5), projected rates of sea-level rise by 2150 are likely to exceed those observed at any time in the past 8,000 years, emphasizing the unprecedented nature of future sea-level rise and the urgent need for mitigation and adaptation.

Our knowledge about regional sea-level change in Asia relies on numerous publications investigating post-LGM RSL change. However, some earlier studies employed approaches that are now considered outdated and limited by the precision of techniques available by then. This includes less accurate determinations of sample elevation, geographic location, and sea-level indicator identification, which introduce substantial uncertainty when evaluated under current standardized frameworks. For example, some early RSL reconstructions lack precise sample location information and do not include supporting microfossil, geochemical, or biological analysis to verify the indicative meaning of the sampled materials, relying instead on visual or subjective interpretations (e.g., classifying a sample as saltmarsh without clear identification based on laboratory analysis). Such records may need to be conservatively reclassified as limiting data rather than SLIPs, or in some cases, excluded entirely accordingly to updated protocol (Khan et al. 2019). Nevertheless, these earlier studies continue to offer valuable contextual information and serve as useful references for guiding future work in the same or adjacent regions.

There are many opportunities for advancing sea-level research in Asia. Two of the most pressing needs are the systematic compilation of RSL data and the reconstruction of high-resolution and high-precision RSL records, particularly from key areas (e.g., sensitive to certain GIA parameters). Refining and expanding these datasets will enhance our understanding of the regional sea-level change and improve our ability to disentangle the contribution from various driving processes. Notably, Asia as a far-field region with minimum land isostatic deformation due to GIA, could provide valuable constraint on ice-equivalent sea level and thus has significant potential for reducing the large uncertainty associated with Antarctic deglaciation history. The limited understanding of Antarctic ice loss and it driving mechanisms remains a major contributor to the uncertainty in global sea-level projections. Another key research opportunity lies in improving estimates of VLM across Asia, especially along the coastlines of major cities. As VLM can substantially affect the local and regional sea-level projections, robust VLM assessments are essential for generating accurate projections and informing effective coastal mitigation and adaptation strategies. Additionally, assessing coastal hazards under rising sea levels is also an important direction for future research. It is necessary to evaluate how sea-level rise may exacerbate existing hazards and potentially generate new ones. Interdisciplinary approaches can reveal new insights, for example, exploring the impact of sea-level rise on marine biodiversity, such as nesting habitats of sea turtles.

Acknowledgments

Tanghua Li was supported by the Singapore Ministry of Education Academic Research Fund MOE2019-T3-1-004 and Project No. 36.9 "The Asia Sea-Level Knowledge Hub (ASK-Hub)”, officially endorsed by the United Nations Educational, Scientific and Cultural Organization (UNESCO) under the UN Decade of Ocean Science for Sustainable Development 2021-2030. This research is conducted in part using the research computing facilities and/or advisory services offered by Information Technology Services, the University of Hong Kong.

References

Amante C, Eakins BW (2009) ETOPO1 arc-minute global relief model: procedures, data sources and analysis

Chua S, Switzer AD, Li T, et al (2021) A new Holocene sea-level record for Singapore. Holocene 31:1376–1390

Church JA, Clark PU, Cazenave A, et al (2013) Sea level change

Engelhart SE, Peltier WR, Horton BP (2011) Holocene relative sea-level changes and glacial isostatic adjustment of the US Atlantic coast. Geology 39:751–754. https://doi.org/10.1130/G31857.1

Fox-Kemper B, Hewitt HT, Xiao C, et al (2021) Ocean, cryosphere, and sea level change. In: Climate Change 2021: The Physical Science Basis. Contribution of Working Group I to the Sixth Assessment Report of the Intergovernmental Panel on Climate Change. Cambridge University Press, pp 1211–1361

Gregory JM, Griffies SM, Hughes CW, et al (2019) Concepts and terminology for sea level: Mean, variability and change, both local and global. Surv Geophys 40:1251–1289

Hammond WC, Blewitt G, Kreemer C, Nerem RS (2021) GPS imaging of global vertical land motion for studies of sea level rise. J Geophys Res Solid Earth 126:e2021JB022355-e2021JB022355

Hanebuth T, Stattegger K, Grootes PM (2000) Rapid flooding of the Sunda Shelf: a late-glacial sea-level record. Science (1979) 288:1033–1035

Horton BP, Kopp RE, Garner AJ, et al (2018) Mapping sea-level change in time, space, and probability. Annu Rev Environ Resour 43:481–521

Kelsey HM, Engelhart SE, Pilarczyk JE, et al (2015) Accommodation space, relative sea level, and the archiving of paleo-earthquakes along subduction zones. Geology 43:675–678

Khan NS, Horton BP, Engelhart S, et al (2019) Inception of a global atlas of sea levels since the Last Glacial Maximum. Quat Sci Rev 220:359–371

Kim HL, Li T, Kalsi N, et al (2023) Prehistoric human migration between Sundaland and South Asia was driven by sea-level rise. Commun Biol 6:150

Kopp RE, Kemp AC, Bittermann K, et al (2016) Temperature-driven global sea-level variability in the Common Era. Proceedings of the National Academy of Sciences 113:E1434–E1441

Kuchar J, Milne G, Latychev K (2019) The importance of lateral Earth structure for North American glacial isostatic adjustment. Earth Planet Sci Lett 512:236–245

Lambeck K, Rouby H, Purcell A, et al (2014) Sea level and global ice volumes from the Last Glacial Maximum to the Holocene. Proceedings of the National Academy of Sciences 111:15296–15303. https://doi.org/10.1073/pnas.1411762111

Latychev K, Mitrovica JX, Tromp J, et al (2005) Glacial isostatic adjustment on 3-D Earth models: a finite-volume formulation. Geophys J Int 161:421–444

Li T, Chua S, Tan F, et al (2023) Glacial Isostatic Adjustment modelling of the mid-Holocene sea-level highstand of Singapore and Southeast Asia. Quat Sci Rev 319:108332

Li T, García-Artola A, Shaw TA, et al (2024) Vertical land motion is underestimated in sea-level projections from the Oka estuary, northern Spain. Sci Rep 14:31302

Li T, Khan NS, Baranskaya A V, et al (2022) Influence of 3D Earth Structure on Glacial Isostatic Adjustment in the Russian Arctic. J Geophys Res Solid Earth 127:e2021JB023631-e2021JB023631

Li T, Wu P (2019) Laterally heterogeneous lithosphere, asthenosphere and sub-lithospheric properties under Laurentia and Fennoscandia from Glacial Isostatic Adjustment. Geophys J Int 216:1633–1647

Li T, Wu P, Wang H, et al (2020) Uncertainties of Glacial Isostatic Adjustment model predictions in North America associated with 3D structure. Geophys Res Lett e2020GL087944-e2020GL087944

Lin Y, Hibbert FD, Whitehouse PL, et al (2021) A reconciled solution of Meltwater Pulse 1A sources using sea-level fingerprinting. Nat Commun 12:1–11

Majewski JM, Meltzner AJ, Switzer AD, et al (2022) Extending Instrumental Sea-Level Records Using Coral Microatolls, an Example From Southeast Asia. Geophys Res Lett 49:e2021GL095710-e2021GL095710

Mitrovica JX, Milne GA (2002) On the origin of late Holocene sea-level highstands within equatorial ocean basins. Quat Sci Rev 21:2179–2190

Mitrovica JX, Peltier WR (1991) On postglacial geoid subsidence over the equatorial oceans. J Geophys Res Solid Earth 96:20053–20071

Mitrovica JX, Tamisiea ME, Davis JL, Milne GA (2001) Recent mass balance of polar ice sheets inferred from patterns of global sea-level change. Nature 409:1026–1029

Ng T, Garner G, Weeks JH, et al (2025) Robust sea-level projections for Singapore by 2100 and 2150. J Geophys Res Oceans 130:e2024JC021840

Nicholls RJ, Cazenave A (2010) Sea-level rise and its impact on coastal zones. Science (1979) 328:1517–1520

Peltier WR, Argus DF, Drummond R (2015) Space geodesy constrains ice age terminal deglaciation: The global ICE-6G_C (VM5a) model. J Geophys Res Solid Earth 120:450–487

Peltier WR, Wu PP-C, Argus D, et al (2022) Glacial Isostatic Adjustment: Physical Models and Observational Constraints. Reports on Progress in Physics

Peng D, Ng G, Feng L, et al (2024) Coastal vertical land motion across Southeast Asia derived from combining tide gauge and satellite altimetry observations. Science of Remote Sensing 100176. https://doi.org/https://doi.org/10.1016/j.srs.2024.100176

Samanta D (2025) Sea level change in Asia. In: Sustainable Development Perspectives in Earth Observation. Elsevier, pp 327–344

Shaw TA, Li T, Ng T, et al (2023) Deglacial perspectives of future sea level for Singapore. Commun Earth Environ 4:204

Shennan I, Long AJ, Horton BP (2015) Handbook of sea-level research. John Wiley & Sons

Shirzaei M, Freymueller J, Törnqvist TE, et al (2021) Measuring, modelling and projecting coastal land subsidence. Nat Rev Earth Environ 2:40–58

Steffen H, Wu P (2011) Glacial isostatic adjustment in Fennoscandia---a review of data and modeling. J Geodyn 52:169–204

Tan F, Khan NS, Li T, et al (2023) Holocene relative sea-level histories of far-field islands in the mid-Pacific. Quat Sci Rev 107995

Tay C, Lindsey EO, Chin ST, et al (2022) Sea-level rise from land subsidence in major coastal cities. Nat Sustain 1–9

Velay-Vitow J, Peltier WR, Stuhne GR, Li T (2024) The hemispheric origins of meltwater pulse 1B. Geophys J Int 239:1021–1037

Wall JD, Stawiski EW, Ratan A, et al (2019) The GenomeAsia 100K Project enables genetic discoveries across Asia. Nature 576:

Whitehouse PL (2018) Glacial isostatic adjustment modelling: historical perspectives, recent advances, and future directions. Earth surface dynamics 6:401–429

Woodroffe SA, Horton BP (2005) Holocene sea-level changes in the Indo-Pacific. J Asian Earth Sci 25:29–43

Wöppelmann G, Marcos M (2016) Vertical land motion as a key to understanding sea level change and variability. Reviews of Geophysics 54:64–92

Wu P (2004) Using commercial finite element packages for the study of earth deformations, sea levels and the state of stress. Geophys J Int 158:401–408

Xiong H, Zong Y, Li T, et al (2020) Coastal GIA processes revealed by the early to middle Holocene sea- level history of east China. Quat Sci Rev 233:106249. https://doi.org/10.1016/j.quascirev.2020.106249